Bull Earthquake Eng (2016) 14:889–918
DOI 10.1007/s10518-015-9855-6

ORIGINAL RESEARCH PAPER

A capacity curve model for confined clay brick infills

H. Özkaynak[1] · M. Sürmeli[2] · E. Yüksel[3]

Received: 20 May 2015 / Accepted: 8 December 2015 / Published online: 14 December 2015

Abstract Experimental studies have proven that clay brick infills, confined with carbon-fiber-reinforced polymers (CFRP) in reinforced concrete (RC) frames, have some advantages in terms of stiffness, strength, energy dissipation capability and damage intensity. Owing to these advantages, existing infill walls in RC frames may be retrofitted with CFRP strips, especially in low-rise buildings in earthquake-prone areas. There is a gap in the literature concerning their behavior model, for use in structural analysis. A piecewise linear capacity curve model called "DUVAR" is proposed here, which estimates the envelope of force-vs.-displacement hysteresis, depending on the data compiled from the literature and the completed experimental studies. A nonlinear shear spring element is utilized in the model to represent the bare and retrofitted infills. The ultimate shear strength and the corresponding displacement, the ratio of cracking stiffness to initial stiffness, the ratio of ultimate strength to cracking strength, and the ductility ratio are the five key parameters of the model. The model is validated against the experimental results of two sovereign studies. Finally, the model is employed in the performance evaluation of an existing three-story RC building to exemplify its straightforward application.

Keywords Analytical modeling · CFRP retrofitting · Infill wall · Infilled frame · Shear spring

1 Introduction

Infill walls are usually considered non-structural elements, though they may increase the lateral strength, stiffness and energy dissipation capacity of a structure, as well as limiting drift and deformations. However, they may also cause soft story mechanisms, short

✉ E. Yüksel
yukselerc@itu.edu.tr

[1] Department of Civil Engineering, Beykent University, Istanbul, Turkey

[2] Department of Civil Engineering, Istanbul Kültür University, Istanbul, Turkey

[3] Faculty of Civil Engineering, Istanbul Technical University, Istanbul, Turkey

columns and eccentricities in plan and elevation. Dolšek and Fajfar (2008) take a critical conclusion, stating that "infill walls can have a beneficial effect on the structural response, provided that they are placed regularly throughout the structure, and that they do not cause shear failures of columns." Significant seismic performance enhancement can be observed in retrofitted infilled frames, in terms of inter-story drift, lateral load and stiffness capacities, energy dissipation capacity, equivalent damping and observed damages (Özkaynak et al. 2011, 2013).

Polyakov (1960) presented one of the pioneering studies on the seismic response of infilled panels surrounded by RC and steel frames. An equivalent diagonal strut was first proposed for modeling the infill panels. Holmes (1961) suggested that the equivalent strut should have a width equal to 1/3 of the length of the masonry panel. Smith and Carter (1969) related the width of the equivalent diagonal strut to the infill-to-frame-stiffness ratio. Žarnic and Gostic (1997) proposed an elastic, perfectly plastic equivalent strut model for infills, which is known as the "multi-strut model". Chrysostomou et al. (1992) and Hashemi and Mosalam (2006), suggested simplified models based on the equivalent strut approach, which take account of the slip along the interface of the frame and masonry infill. The models use empirically determined correction factors to calculate effective strut dimensions. Dhanasekhar and Page (1986), Mosalam (1996) and Shing and Lotfi (1991) used FEM to predict the general behavior of infilled frames. Madan et al. (1997) proposed a method for computing the in-plane hysteretic force deformation behavior of the masonry infilled frame, based on a tie-and-strut approach, in which the infill is modeled as a combination of three non-parallel struts in each direction of loading. A smooth hysteretic model was developed that uses degrading control parameters for stiffness, strength and slip. Saneinejad (1990) developed an analytical model based on nonlinear FEA and experimental results, taking account of various lower-bound solutions. Saneinejad and Hobbs (1995) developed a method, based on the equivalent diagonal strut approach, for the analysis and design of infilled frames subjected to in-plane forces. This method takes into account the elastoplastic behavior of the infilled frame, considering the limited ductility of the infill wall. Infill aspect ratio, shear stress at the frame-infill interface, and beam and column strength are all accounted for in the method. Smyrou et al. (2011) performed a verification study using the fiber-based FE program and a double-strut nonlinear cyclic model for unreinforced masonry panels. The capability of the model for predicting the cyclic seismic response of the multi-story infilled RC frames was then verified through comparisons with experimental results. Erkoseoglu et al. (2014) proposed a piecewise linear capacity curve, including cracking, maximum and ultimate points based on the experimental data collected from the literature. The defined parameters were verified for unreinforced and confined masonry walls that reasonably matched with the experimental results. This analytical approach was used to conduct a parametric study for the comparison of the behavior of these two distinct types of masonry wall. The concept of simulating the infill with single or multiple diagonal struts under compression is widely accepted as a simple and rational way to describe the influence of the infills on the surrounding frame, and has been adopted in many documents and new guidelines, such as S304.1 (CSA 2004), SEI 41-06 (ASCE 2007), NZSEE (2006) and MSJC (2011).

Although several studies concerning the analytical modeling of masonry infill walls have been completed in the past, only a few of them have concentrated on retrofitted infills. The rationale of this paper is to propose a straightforward empirical model for bare and CFRP-based retrofitted infills made of perforated clay bricks, to be used especially in the performance evaluation of existing low-rise RC buildings in earthquake-prone areas. The scope of the study is based on the literature review and on-hand experimental

consequences. Subsequent to the validation of the proposed empirical model with the results of two sovereign tests, the model is employed in the earthquake performance evaluation of an existing three-story RC building. The main objective of this paper is to generate a piecewise tri-linear capacity curve model to be used as an envelope for load-vs.-displacement hysteresis of perforated clay brick infills without CFRP retrofitting in RC frames.

2 Compilation of the existing data

An assessment of the existing literature demonstrates that there exists a significant number of experimental works which aim to determine the cyclic behavior of the infilled frames. The main characteristics of the specimens selected from the literature are brought together in Table 1. The literature review yields some significant data for the current study, in terms of the estimation of *ultimate displacement* and *strength capacities*, which are represented in columns 8 and 10 of Table 1, respectively. Based on the compiled data, the following conclusions could be drawn:

1. For bare infills, the average drift corresponding to the ultimate strength is in the range of 0.90–1.00 %.
2. For the retrofitted infills, the average drift corresponding to the ultimate strength is in the range of 0.70–1.15 %.

Various equations exist in the literature to determine the *ultimate strength* of infills. The equation proposed in FEMA-356 (2000) for bare infills, and the equation proposed by Triantafillou (1998) for CFRP-based retrofitted infills, are shown on Table 2, along with a definition of their variables.

The equation given in FEMA-356 (2000) to determine the ultimate loading capacity of bare infills is used here for its simplicity. The contribution of CFRP is added to the infill wall capacity. The shear capacity provided by CFRP can be determined from Eq. (1):

$$V = \varepsilon E w t \tag{1}$$

where V is the ultimate shear capacity provided by the CFRP sheet, ε is the ultimate strain, E is the modulus of elasticity of CFRP, and w and t are the width and thickness of CFRP, respectively.

3 The experimental background

A group of 1/3-scale specimens, consisting of infilled and CFRP-retrofitted infilled RC frames, were tested in the Structural and Earthquake Engineering Laboratory at Istanbul Technical University. Two discrete types of retrofitting—namely *cross bracing* and *diamond cross bracing*—were studied, experimentally. The details of the study can be found elsewhere (Yüksel et al. 2009; Özkaynak et al. 2011). The dimensions, reinforcing details and pictures of the tested specimens are presented in Fig. 1. The average compression strength of concrete obtained from the standard cylinder tests was 19 MPa. The yield strength of the reinforcing bars was 420 and 500 MPa for 8 and 6 mm diameters, respectively. Clay hollow bricks with dimensions of 88 × 84 × 57 mm were used in the production of the infill wall, which has an aspect ratio of 1.17. The compression tests

Table 1 Summary of the existing literature

Literature	Number of bays	Number of stories	Infill dimensions (width × height in mm)	Aspect ratio	Brick type Brick dimension (length × width × height in mm)	Parameters	Story displacement corresponding to maximum lateral load (δ_{top} in mm)	Story drift corresponding to maximum lateral load (drift ratio as %)	Maximum lateral strength (F_{top} in kN)
(1)	(2)	(3)	(4)	(5)	(6)	(7)	(8)	(9)	(10)
Mosalam et al. (1998)	1	1	1785 × 926	1.92	¼-Scale Clay brick 99 × 48 × 51	Steel frame without opening	14.01	1.52	18.2
	2	1				Steel frame without opening	11.85	1.28	36
	2	1				Steel frame with opening (305 × 305 mm)	12.31	1.33	42.3
Özcebe et al. (2003)	1	2	1300 × 750	1.73	Clay brick 85 × 75 × 90	RC frame without opening and without CFRP strengthening	12.75	1.7	55.8
	1	2				RC frame without opening and with CFRP strengthening	11.75; 8.55; 20.1; 13.12; 6.6; 6.45	1.49, 1.14, 2.68, 1.75, 0.88, 0.86	64.6; 65.4, 131.5; 118.8; 100.4; 105.7
Altın et al. (2008a)	1	2	1300 × 750	1.73	RC infill wall	Without infill wall	15.07	2.01	13.94 kN
	1	2				With infill wall	2.02; 2.47; 2.17; 2.32; 2.4	0.27; 0.33; 0.29; 0.31; 0.32	156; 82.31; 127.02; 136.53; 165.25

Table 1 continued

Literature	Number of bays	Number of stories	Infill dimensions (width × height in mm)	Aspect ratio	Brick type Brick dimension (length × width × height in mm)	Parameters	Story displacement corresponding to maximum lateral load (δ_{top} in mm)	Story drift corresponding to maximum lateral load (drift ratio as %)	Maximum lateral strength (F_{top} in kN)
(1)	(2)	(3)	(4)	(5)	(6)	(7)	(8)	(9)	(10)
Altın et al. (2008b)	1	1	1300 × 750	1.73	1/3-Scale perforated clay tiles 65 × 95 × 95	Non-retrofitted	3.0	0.4	76.7 kN
	1	1				CFRP-retrofitted	4.27; 6.0; 6.15; 4.12; 3.75; 4.57; 3.75; 3.9; 4.35	0.57; 0.8; 0.82; 0.55; 0.5; 0.61; 0.5; 0.52; 0.58	167.0; 187.2; 200.4; 114.0; 131.5; 139.5; 118.3; 131.0; 142.1
Erdem et al. (2006)	3	2	890 × 850	1.05	Hollow clay block 85 × 69 × 90	With RC infill	7.65	0.9	70.6 kN
	3	2	890 × 1395	0.64	Hollow clay block 85 × 69 × 90	With CFRP-retrofitted infill	9.76 mm	0.7	64.7 kN
Saatcioglu (2003)	1	1	1825 × 1825	1.0	Masonry infill 365 × 240 × 202	Non-retrofitted	18.25 mm	1.0	273 kN
	1	1				CFRP-retrofitted	5.47 mm	0.3	784 kN
Yüksel et al. (2009)	1	1	933 × 800	1.2	Clay Brick 85 × 60 × 85	Non-retrofitted	8.8 mm	1.1	119.9 kN
	1	1				CFRP-retrofitted	8.8; 4.4; 6.4; 8.8	1.1; 0.5; 0.8; 1.1	153.0; 191.8; 137.0; 203.0
Anil and Altin (2007)	1	1	1/3-Scale 1300 × 750	1.73	RC infill wall	RC frame with RC infill and without opening	4.27; 5.85	0.57; 0.78	351.0; 247.9
	1	1				RC frame with partial infills with dowels	9.52; 4.42; 5.55; 8.62; 9.60; 5.17	1.27; 0.59; 0.74; 1.15; 1.28; 0.69	88.6; 150.3; 193.8; 155.9; 126.4; 173.1

Table 1 continued

Literature	Number of bays	Number of stories	Infill dimensions (width × height in mm)	Aspect ratio	Brick type Brick dimension (length × width × height in mm)	Parameters	Story displacement corresponding to maximum lateral load (δ_{top} in mm)	Story drift corresponding to maximum lateral load (drift ratio as %)	Maximum lateral strength (F_{top} in kN)
(1)	(2)	(3)	(4)	(5)	(6)	(7)	(8)	(9)	(10)
Almusallam and Al-Salloum (2007)	1	1	2100 × 1550	1.35	Clay brick 400 × 100 × 200	Non-retrofitted	9.61	0.62	417 kN
	1	1				CFRP-retrofitted	14.26; 19.22	0.92; 1.24	442; 371 kN
Kakaletsis and Karayannis (2009)	1	1	1/3-Scale 1200 × 800	1.5	Clay brick 93 × 60 × 60	RC frame without opening	8.00	1.0	80 kN
	1	1				RC frame with opening	7.15; 6.4	1.1; 1.1	65.0; 58 kN
Pujol and Fick (2010)	2	3	Full-scale 5641 × 3050	1.85	Clay brick 90 × 55 × 195	Infilled	46	1.5	4540 kN

Table 2 Shear strength of the infill and retrofitted infill wall

Reference	Case	Equations	Parameters
Mainstone (1971) and FEMA-356 (2000)	Bare infill wall	Corner crushing failure mode $a = 0.175\ (\lambda_1\ h_{col})^{-0.4}\ r_{inf}$ $\lambda_1 = \left[\frac{E_{me} t_{inf} \sin 2\theta}{4 E_{fe} I_{col} h_{inf}}\right]^{1/4}$ Bed joint failure mode $Q_{CE} = V_{ine} = A_{ni} f_{vie}$	a = Equivalent strut thickness λ_1 = Coefficient used to determine equivalent width of infill strut h_{col} = Column height between centerlines of beams r_{inf} = Diagonal length of infill panel E_{me} = Expected modulus of elasticity of material t_{inf} = Thickness of infill panel and equivalent strut θ = Angle whose tangent is the infill height-to-length aspect ratio E_{fe} = Expected modulus of elasticity of frame material I_{col} = Moment of inertia of column h_{inf} = Height of infill panel A_{ni} = Area of net mortared/grouted section across infill panel f_{vie} = Expected shear strength of masonry infill V_{ine} = Expected infill shear strength
Triantafillou (1998)	CFRP-based retrofitted infill wall	$V_{Rd} = f_{vk}\ t\ d + 0.9\ d\ \rho_{FRP}\ E_{FRP}\ r\ \varepsilon_{FRP,u}\ t$ $r{\cdot}\varepsilon_{FRP,u} = 0.0119 - 0.0205 \times (\rho_{FRP} E_{FRP}) + 0.0104(\rho_{FRP} E_{FRP})^2$	V_{Rd} = Shear capacity of masonry wall f_{vk} = Shear strength obtained from the triplet shear tests t = Wall length $d = 0.8\ l$ effective depth l = Wall thickness ρ_{FRP} = FRP ratio E_{FRP} = Elasticity modulus of FRP r = A factor depending on the failure mode of the FRP $\varepsilon_{FRP,u}$ = Ultimate tensile strain of FRP

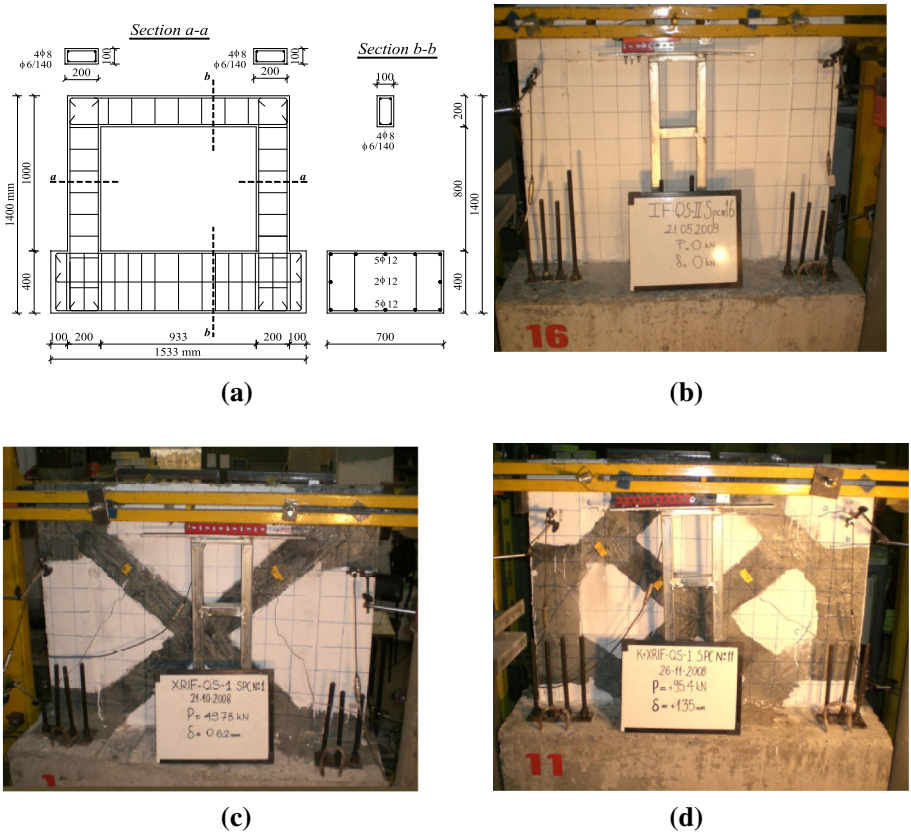

Fig. 1 Dimensions, reinforcing details and pictures of the specimens. **a** Dimensions and reinforcing retails. **b** Infilled frame. **c** Cross braced frame. **d** Diamond cross braced frame

performed on 350 × 350 mm wall mock-ups yielded compression strengths of 5.0 and 4.1 MPa in two perpendicular directions. The diagonal shear tests performed on the same-sized wall specimen resulted in 0.95 MPa of shear strength. A unidirectional type of CFRP sheet was used in the retrofitting. As per the technical data provided by the manufacturer, the unit weight of the CFRP was 300 g/m^2, the fiber density was 1.79 g/cm^3 and the modulus of elasticity of the CFRP was 230 GPa. Tensile strength and ultimate elongation capacities were 3900 MPa and 1.5 %, respectively. For the wall mock-ups that were retrofitted with CFRP, the average compressive and shear strengths were 7.5 and 1.8 MPa, respectively. Additionally, the modulus of elasticity was determined as 7600 MPa.

A servo-controlled, 280 kN-capacity hydraulic actuator, aligned to the center of the beam, was utilized to generate cyclic displacement reversals in quasi-static (QS) tests (Fig. 2). The rigid foundation of the specimen was fixed to the strong floor.

The general damage patterns and envelopes of force–displacement hysteresis obtained from the QS tests are presented in Fig. 3. The critical events, such as first cracking in RC members, first diagonal cracking in infill, rupture or tearing of CFRP, and buckling of re-bar, are designated on the curves.

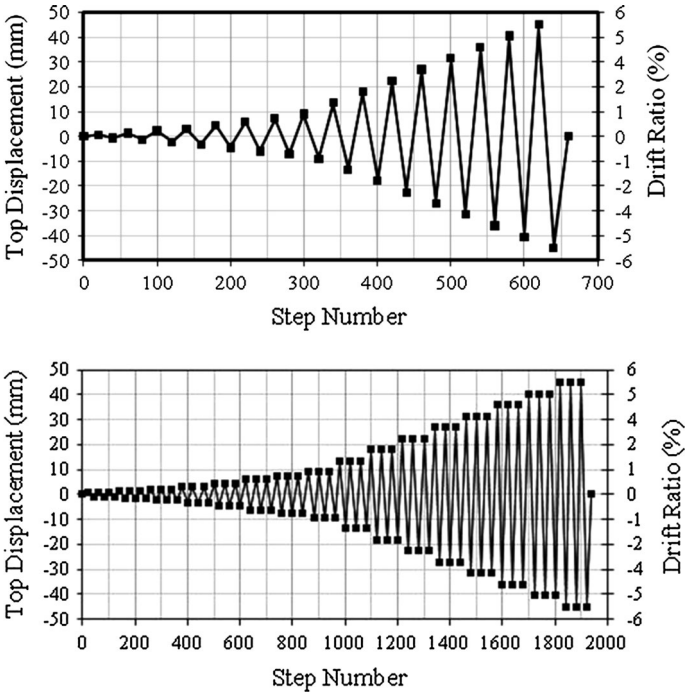

Fig. 2 One-cycle and three-cycle displacement protocols used in QS tests

Some of the damage indications and corresponding drifts are compiled in Table 3.

Based on Tables 2 and 3, the generalized drift corresponding to the ultimate shear strength could be proposed as given in Table 4.

According to the experimental data extracted from the unidirectional strain gauge measurements in the QS tests, the CFRP tears when the strain reaches 0.6 %. This critical value was used in the calculation of the CFRP's contribution to the ultimate shear strength of the infill wall (Eq. 1).

4 Development of the "DUVAR" capacity curve model

To develop the capacity curve model that we have called "DUVAR", three sets of piecewise linear envelopes were generated from the QS test results. The breaking points on the envelopes correspond to the cracking, maximum and ultimate strength, and displacement couples (Figs. 4, 5, 6).

The contribution of the bare and CFRP-retrofitted infills to the system behavior is represented by the proposed "DUVAR" model (Fig. 7). The model consists of three piecewise linear segments: namely, *pre-cracking*, *post-cracking* and *descending branches*. The self-determining parameters of the model are V_{max}, δ_{max}, β, ϕ and μ, which appear in the rectangles in Fig. 7. These parameters are decisive in expressing *initial stiffness*, *effective stiffness* and *ductility*.

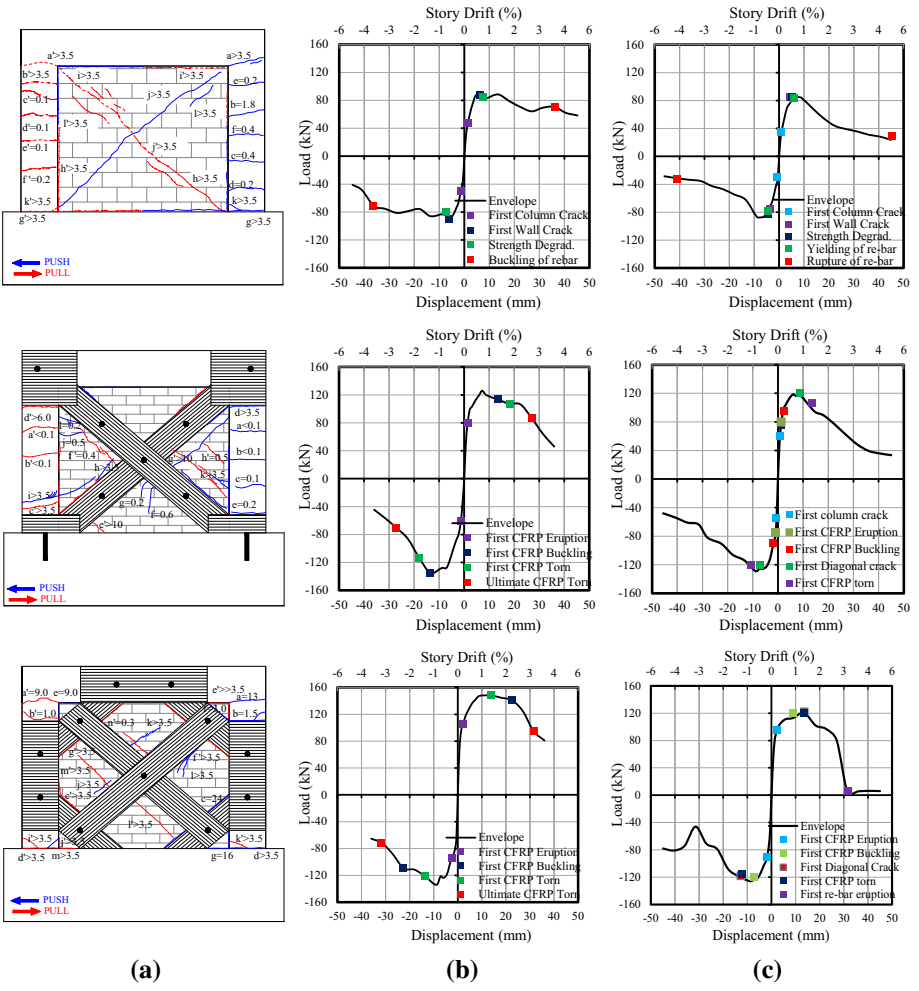

Fig. 3 QS test results. **a** Damage pattern. **b** 1-cycle protocol. **c** 3-Cycle protocol

The definitions of all the variables used in the "DUVAR" model are listed in Table 5. The lines corresponding to the self-determining parameters are indicated with gray shading.

The numerical assignments to the parameters are presented in Tables 6 and 7 for the one-cycle and three-cycle QS tests, respectively.

ϕ, β and μ are unitless parameters which were generated to characterize imperative features of infills without CFRP strips. The overall values which are deliberated as the average of pushing and pulling directions are presented in Table 8.

The ultimate shear strength of the infill (V_{max}) was determined using the FEMA-356 (2000) approach, as given in Table 2. Based on the results of the experimental study and the literature review summarized in Table 1, the drift ratio (δ_{max}/h) corresponding to the ultimate shear was assigned at 1.0 % for bare infills and 1.20 % for the retrofitted infills (see Table 4).

Table 3 Critical drifts (%) determined from QS tests

Event	Infilled frame		Cross-braced frame		Diamond cross-braced frame	
	One-cycle	Three-cycle	One-cycle	Three-cycle	One-cycle	Three-cycle
Flexural cracks on columns	0.15	0.15	0.15	0.08	0.15	0.08
Yielding of longitudinal reinforcement	0.80	1.00	0.60	0.45	0.40	0.30
Separation of infill from RC members	0.25	0.25	0.25	0.15	0.25	0.15
Diagonal cracking	0.70	0.50	0.70	1.00	1.50	0.35
Strength degradation	0.63	0.67	0.96	0.69	1.97	1.58
Corner crushing on infill wall	2.00	2.00	3.00	2.50	3.50	3.00
Tearing of CFRP	N/A	N/A	2.00	1.50	2.50	2.00

Table 4 The generalized drifts corresponding to the ultimate shear strength

Frame	Δ_{max} (%)
Bare infilled	1.00
Cross-braced	1.10
Diamond cross-braced	1.20

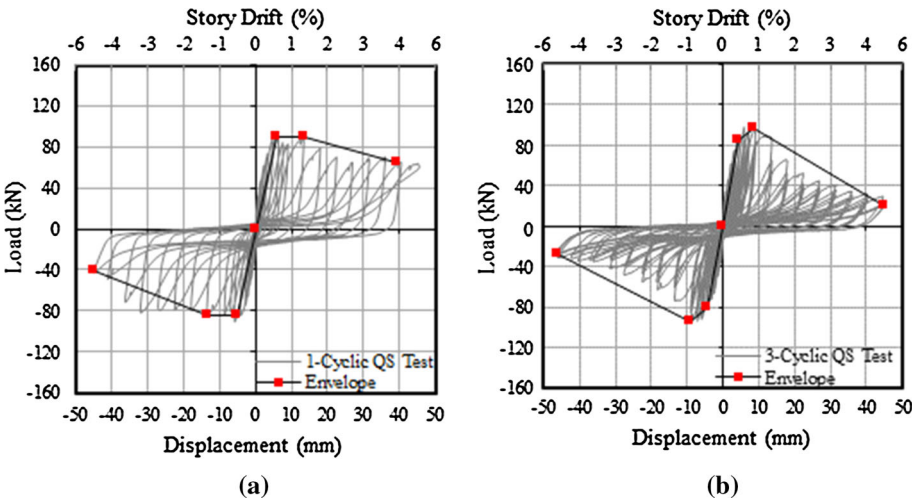

Fig. 4 Envelopes of infilled frames. **a** 1-Cycle QS. **b** 3-Cycle QS

In order to generate the proposed model, the following steps should be traced:

Step 1: The ultimate shear strength (V_{max}) of the infill wall without CFRP retrofitting is determined according to FEMA-356 (2000) (see Table 2)

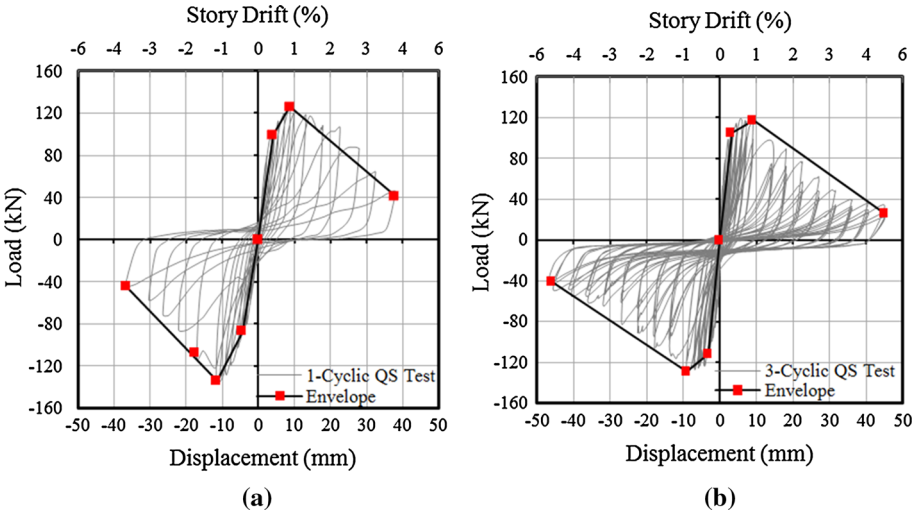

Fig. 5 Envelopes of cross-braced frames. **a** 1-Cycle QS. **b** 3-Cycle QS

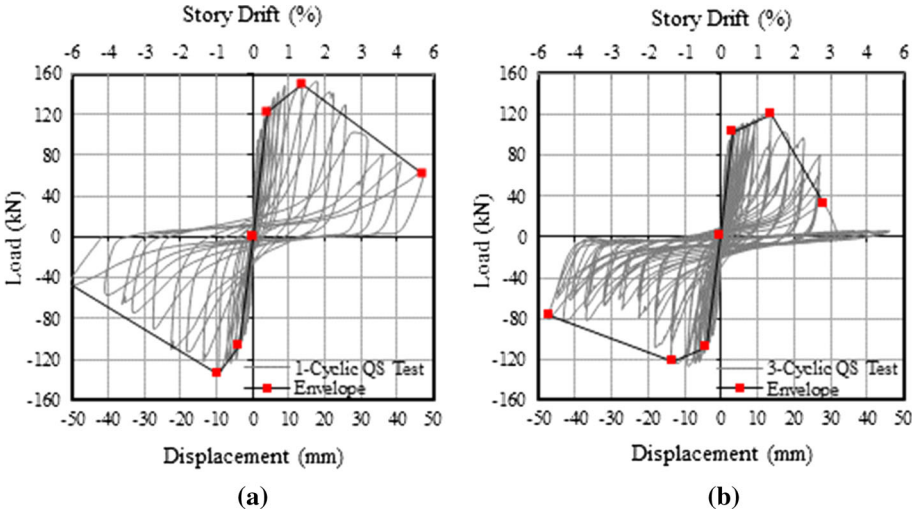

Fig. 6 Envelopes of diamond cross-braced frames. **a** 1-Cycle QS. **b** 3-Cycle QS

Step 2: The drift ratio (δ_{max}/h) corresponding to the V_{max} is taken from Table 4. The displacement (δ_{max}) is calculated by multiplying the drift ratio by the story height (h) (Eq. 2)

$$\delta_{max} = \Delta_{max} \times h \tag{2}$$

Step 3: The secant stiffness (K_{sec}) is calculated by dividing the ultimate shear strength (V_{max}) by the corresponding displacement (δ_{max}) (Eq. 3)

$$K_{sec} = V_{max}/\delta_{max} \tag{3}$$

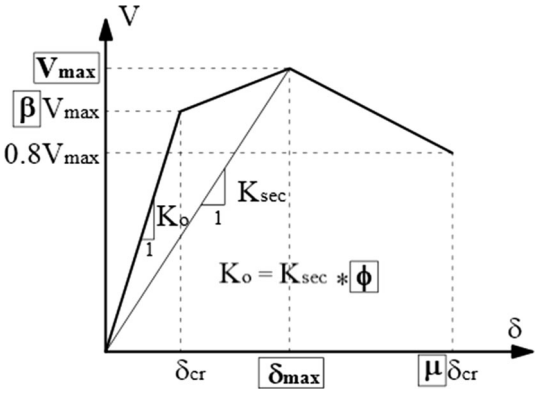

Fig. 7 Parameters of the "DUVAR" capacity curve model

Table 5 Variables of the proposed "DUVAR" capacity curve model

Parameter	Definition
V_{max}	The ultimate shear capacity of the infill
δ_{max}	The displacement corresponding to V_{max}
δ_{cr}	The displacement at which the first cracking was observed
K_{sec}	The ratio of V_{max} to δ_{max}
K_o	The ratio of V_{cr} to δ_{cr}
ϕ	The ratio of initial stiffness to secant stiffness ($\phi = K_o/K_{sec}$)
β	The ratio of V_{cr} to V_{max} ($\beta = V_{cr}/V_{max}$)
γ	The ratio of V_u to V_{max} ($\gamma = V_u/V_{max}$)
μ	The ductility ratio δ_u to δ_{cr}
θ	The slope of descending branch ($\theta = (V_{max} - V_u)/(\delta_u - \delta_{max})$)
α	The post-yield flexural stiffness ratio ($\alpha = (V_{max} - V_{cr})/(\delta_{max} - \delta_{cr})$) $(1/K_o)$)

Table 6 Numerical assignments to the model variables for the one-cycle QS tests

Specimen type		V_{cr} kN	V_{max} kN	V_u kN	δ_{cr} mm	δ_{max} mm	δ_u mm	K_{sec} kN/mm	K_o kN/mm	ϕ –	β –	μ –
Infilled frame	+	89	90	71	3.0	13.5	30.0	6.6	29.7	4.50	1.00	8.3
	–	84	85	72	3.0	13.3	21.3	6.4	28.0	4.40	0.98	7.3
Cross-braced frame	+	100	126	101	1.8	8.7	17.5	14.5	55.6	3.80	0.79	9.7
	–	87	134	107	2.0	11.5	17.5	11.7	43.5	3.75	0.65	6.3
Diamond cross-braced frame	+	123	150	120	2.5	13.6	24.0	11.0	49.2	4.46	0.82	8.0
	–	108	134	107	2.7	9.3	22.5	14.3	39.8	2.77	0.80	7.4

Step 4: The pre-cracking stiffness (K_0) is calculated by multiplying the secant stiffness (K_{sec}) by ϕ, which is given in Table 8 (Eq. 4)

$$K_0 = \phi \times K_{sec} \tag{4}$$

Table 7 Numerical assignments to the model variables for the three-cycle QS tests

Specimen type		V_{cr} kN	V_{max} kN	V_u kN	δ_{cr} mm	δ_{max} mm	δ_u mm	K_{sec} kN/mm	K_o kN/mm	ϕ –	β –	μ –
Infilled frame	+	75	98	78	2.0	8.8	18.0	11.0	37.5	3.37	0.88	9.0
	–	81	95	76	2.0	8.9	17.3	10.7	40.3	3.78	0.84	9.0
Cross-braced frame	+	105	117	94	2.0	9.1	17.5	12.9	52.5	4.05	0.89	8.5
	–	112	129	103	1.8	9.1	17.5	14.2	62.1	4.38	0.86	10.0
Diamond cross-braced frame	+	102	120	96	2.5	13.6	17.5	8.8	40.9	4.62	0.85	8.0
	–	108	122	98	2.5	13.1	22.5	9.4	43.2	4.61	0.88	12.0

Table 8 The overall unitless parameters of the proposed "DUVAR" capacity curve model

Specimen type	ϕ		β		μ	
	One-cycle	Three-cycle	One-cycle	Three-cycle	One-cycle	Three-cycle
Infilled frame	5.0	4.0	0.99	0.86	7.0	6.0
Cross-braced frame	4.0	5.0	0.72	0.87	8.0	8.0
Diamond cross-braced frame	4.0	5.0	0.81	0.86	8.0	8.0

Step 5: The cracking strength (V_{cr}) is calculated by multiplying the ultimate strength (V_{max}) by β, which is given in Table 8 (Eq. 5)

$$V_{cr} = \beta \times V_{max} \tag{5}$$

Step 6: The cracking displacement (δ_{cr}) is calculated by dividing the cracking strength (V_{cr}) by the pre-cracking stiffness (K_0) (Eq. 6)

$$\delta_{cr} = V_{cr}/K_0 \tag{6}$$

Step 7: The ultimate displacement (δ_u) is determined by multiplying the cracking displacement (δ_{cr}) by μ, given in Table 8 (Eq. 7)

$$\delta_u = \mu \times \delta_{cr} \tag{7}$$

Step 8: The strength (V_u) corresponding to the ultimate displacement is calculated as a 20 % drop in V_{max} (Eq. 8)

$$V_u = 0.80 \times V_{max} \tag{8}$$

5 Verification of the "DUVAR" capacity curve model

The verification of the proposed "DUVAR" capacity curve model was accomplished for three discrete cases. The first and second cases involved QS and pseudo-dynamic tests (PsD), respectively, of the 1/3-scale one-bay/one-story infilled frames. The third example

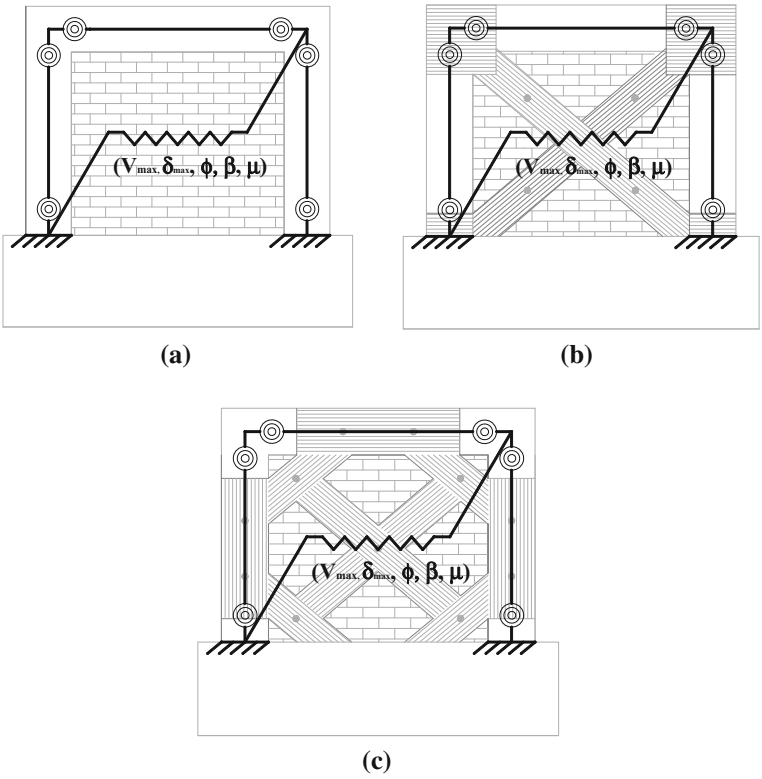

Fig. 8 Analytical models of one-bay/one-story 1/3-scale specimens. **a** Infilled frame. **b** Cross braced frame. **c** Diamond cross braced frame

related to the ½-scale one-bay/two-story infilled RC frame. For all cases, the analytically obtained force-versus-displacement curves were compared with the experimental results.

The *nonlinear spring-type link element*, which is available in most analysis packages (such as SAP 2000), was used for the application of the infill model. The nonlinear behavior of the RC members was represented by the plastic hinges assigned at both ends of the members. The sectional analysis of the RC members was performed by XTRACT (2006).

Material nonlinearity is accounted for in the pushover analysis, in which lateral displacement increments were applied to story levels.

Case 1 QS tests of one-bay/one-story 1/3-scale specimens

The analytical model consists of three frame elements which represent the nonlinear behavior of columns and beams, and a nonlinear spring that represents the nonlinear behavior of the infill without CFRP retrofitting (Fig. 8).

The characteristic points of the bi-linear moment–curvature relations generated for the plastic hinges defined at both ends of the frame elements are given in Table 9.

The terms of the bare and retrofitted infill capacity curves for the *one-cycle* and *three-cycle* QS tests were determined using the procedure defined above (Fig. 7). The overall

Table 9 Characteristic points of the plastic hinges defined on the RC members

		Column	Beam
Moment (kN mm)			
Yielding	M_y	6558.0	10360.0
Ultimate	M_u	7633.0	10150.0
Curvature (1/mm)			
Yielding	χ_y	1.6×10^{-5}	1.9×10^{-5}
Ultimate	χ_u	5.8×10^{-4}	4.7×10^{-4}

Table 10 Characteristic points of "DUVAR" for Case #1 and Case #2

Step	Parameter	Unit	Infill wall		Cross-braced infill wall		Diamond cross-braced infill wall	
			One-cycle	Three-cycle	One-cycle	Three-cycle	One-cycle	Three-cycle
1	V_{max}	kN	53.55	53.55	92.20	92.20	109.71	100.82
2	δ_{max}	mm	9.00	9.00	9.90	9.90	10.80	10.80
3	K_{sec}	kN/mm	5.95	5.95	9.31	9.31	10.15	10.15
3–4	ϕ	–	5.00	4.00	4.00	5.00	4.00	5.00
4	K_o	kN/mm	29.75	23.80	37.25	46.56	40.63	50.80
4–5	β	–	0.99	0.86	0.72	0.87	0.81	0.86
5	V_{cr}	kN	53.02	46.05	66.40	80.67	88.87	94.90
6	δ_{cr}	mm	1.78	1.93	1.78	1.73	2.18	1.86
6–7	μ	–	7.00	6.00	8.00	8.00	8.00	8.00
7	δ_u	mm	12.47	11.61	14.25	13.86	17.49	14.94
8	V_u	kN	49.50	48.40	78.19	82.47	93.81	98.64

parameters listed in Table 8 were used in the determination of the model variables. The calculated model variables are given in Table 10.

The force-vs.-displacement curves obtained from the pushover analyses for the three cases—namely, the infilled frame, cross-braced frame and diamond cross-braced frame—were compared with the backbone curves of the corresponding experimental hystereses (Fig. 9).

It could be concluded that the force-versus-displacement curves obtained from the pushover analyses are close enough to represent the experimental results. The initial stiffness, load-bearing capacity and slope of the descending branch fit rather well with the test results.

Case 2 PsD tests of one-bay/one-story 1/3-scale specimens

Details of the PsD testing can be found elsewhere (Altın et al. 2008a). The acceleration record shown in Fig. 10 was used in the PsD tests. The record was multiplied by two coefficients (0.5 and 1.5) to scale down and up to reach 0.2 and 0.6 g records, respectively.

The analytical force–displacement curves are illustrated in Fig. 11, together with the force–displacement hysteresis obtained from the PsD tests, which represents the results of

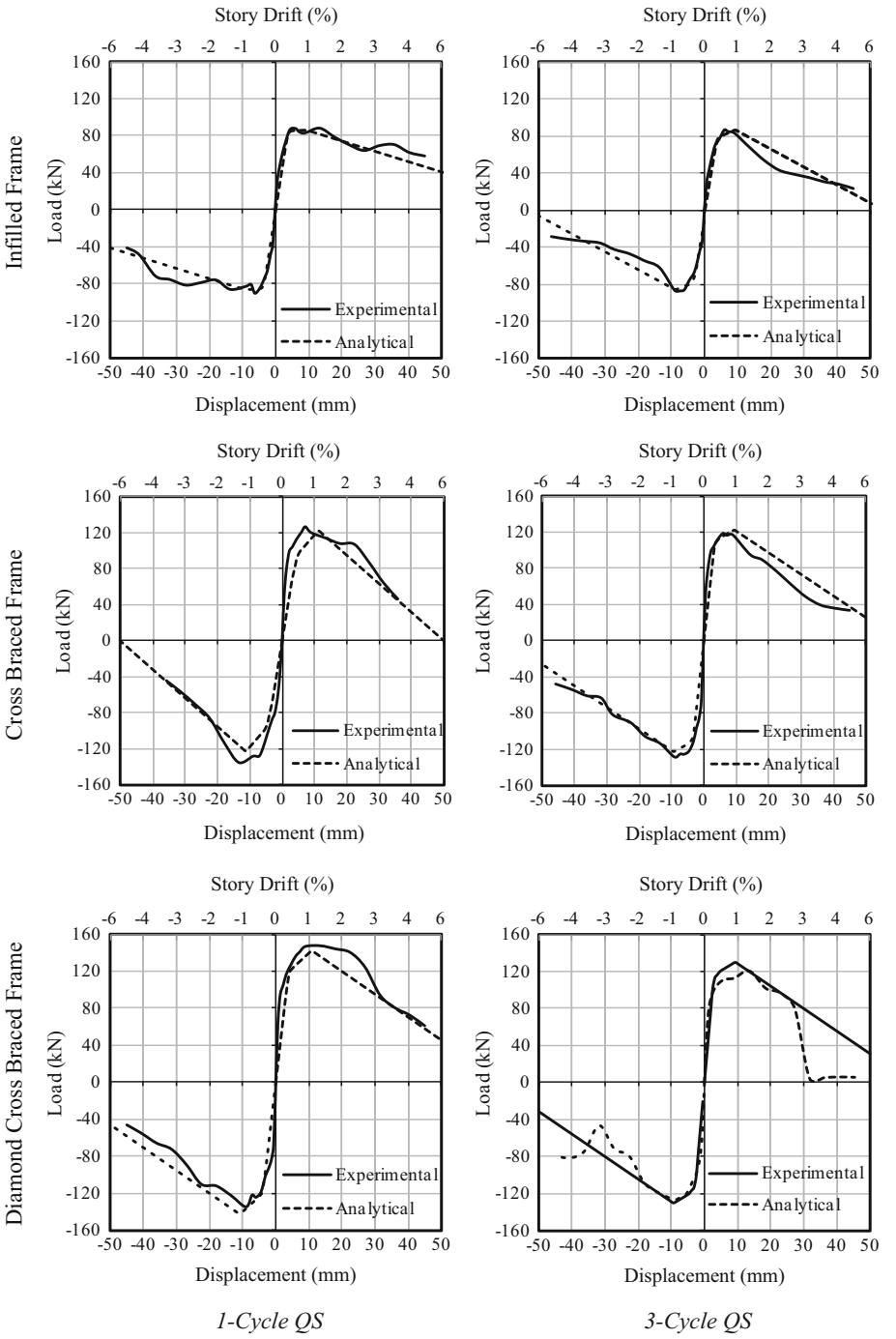

Fig. 9 Comparisons of the analytical results with the experimental backbone curves

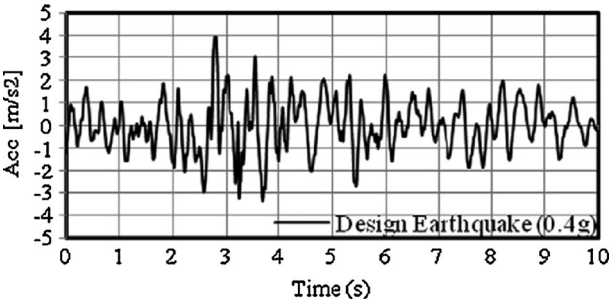

Fig. 10 The acceleration record used in the PsD tests

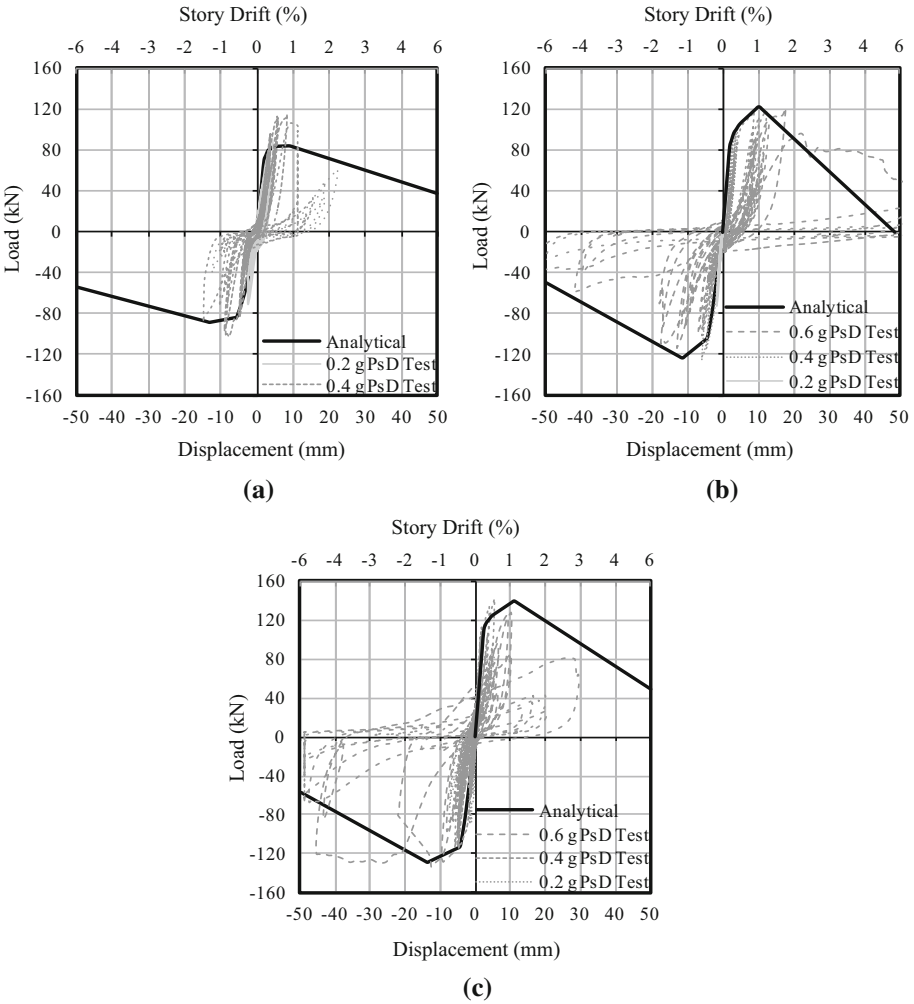

Fig. 11 Comparison of theoretical results with the PsD test results. **a** Infilled frame. **b** Cross braced frame. **c** Diamond cross braced frame

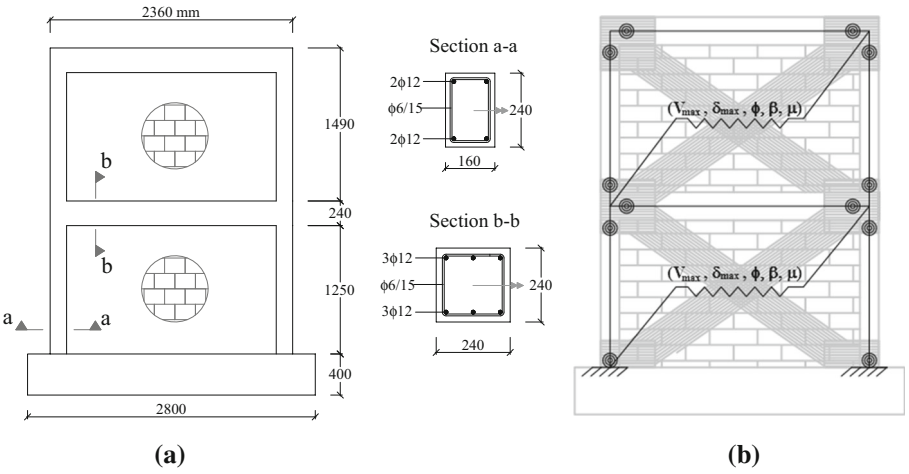

Fig. 12 The dimensions and reinforcement details of the specimen (all dimensions are in mm). **a** Dimensions and reinforcement details. **b** Analytical model

three successive runs: namely, 0.2, 0.4 and 0.6 g. In general, the analytical results converge with the test results in terms of initial stiffness, ultimate strength and descending branches.

Case 3 One-bay/two-story ½-scale specimens

A number of one-bay/two-story ½-scale RC frames were tested in the Structural and Earthquake Engineering Laboratory at ITU, within the framework of a research project (Karadogan et al. 2003). The experimental results obtained from the bare, infilled and cross-braced frame tests were used here to evaluate the success of the "DUVAR" model. The dimensions and reinforcement details of the specimens are demonstrated in Fig. 12a. No confinement reinforcement existed in or around the beam-column connections.

The yielding and ultimate strengths of longitudinal reinforcement in the RC members used were 270 and 290 MPa, respectively. The compression strength for the concrete was 14, 11 and 10 MPa, obtained from 150 × 300 mm standard cylinder tests for *bare*, *infilled* and *cross-braced frames*, respectively.

The clay perforated brick used in the infill wall had dimensions of 88 × 84 × 56 mm. Both sides of the infill wall were plastered 10 mm thick. Compression tests performed on the 350 × 350 mm brick infill mock-ups yielded a compression strength of 5.0 and 4.1 MPa, in two perpendicular directions. The tests performed on the same-sized specimens resulted with 0.95 MPa shear strength. The unit weight and fiber density of the CFRP used were 300 g/m^2 and 1.79 g/cm^3, respectively. Furthermore, the modulus of elasticity, tensile strength and ultimate elongation capacity of CFRP were 230 GPa, 3900 MPa and 1.5 %, respectively.

The specimens were subjected to constant vertical and varying lateral forces. In the lateral direction, reversal displacement cycles were applied at various ductility levels. The lateral loading system seen in Fig. 13 could handle the force distribution ratio between the lower and upper stories being 1:2.

The analytical model, which consists of six beam-columns and two shear spring-type nonlinear elements, is illustrated in Fig. 12b. The characteristic points of bi-linear

Fig. 13 One-bay/two-story infilled frame tests (Karadogan et al. 2003). **a** Testing set-up. **b** Damage condition

moment–curvature relations generated for the plastic hinges defined at both ends of the RC members are listed in Table 11.

The "DUVAR" model parameters prepared for the bare and retrofitted infills are tabulated in Table 12.

The base-shear-versus-top-displacement relations obtained through nonlinear static analysis, in which constant vertical and incremental lateral displacements were used, were compared with the backbone curves of the experimental hysteresis (Fig. 14).

For each distinct case, the initial stiffness, ultimate strength and descending branch are comparable between the experimental and analytical results. Hence, the "DUVAR" model can represent the effects of bare and retrofitted infill on the general response.

Table 11 Characteristic points of the plastic hinges defined on RC members

		Column	Beam
Moment (kN m)			
Yielding	M_y	10.74	17.77
Ultimate	M_u	10.74	17.77
Curvature (1/m)			
Yielding	χ_y	0.005572	0.002731
Ultimate	χ_u	0.005572	0.002731

Table 12 Characteristic points of the "DUVAR" model for Case *#3*

Step	Parameter	Unit	Infilled frame	Cross-braced frame
1	V_{max}	kN	123.46	188.30
2	Δ_{max}	mm	13.70	15.07
3	K_{sec}	kN/mm	9.02	12.49
3–4	ϕ	–	5.00	5.00
4	K_o	kN/mm	45.09	78.45
4–5	β	–	0.98	0.72
5	V_{cr}	kN	106.18	164.76
6	δ_{cr}	mm	2.30	2.10
6–7	μ	–	4.74	6.26
7	δ_u	mm	16.49	17.36
8	V_u	kN	98.77	150.64

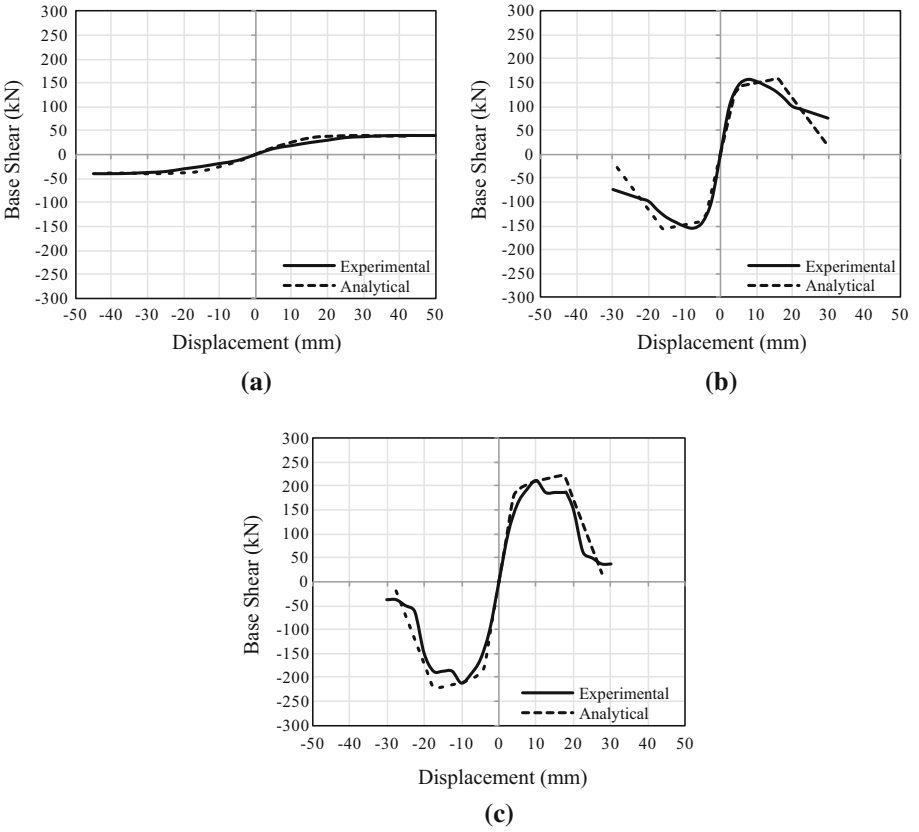

Fig. 14 Theoretical and experimental results of the bare frame and infilled frame. **a** Bare frame. **b** Infilled frame. **c** Cross braced frame

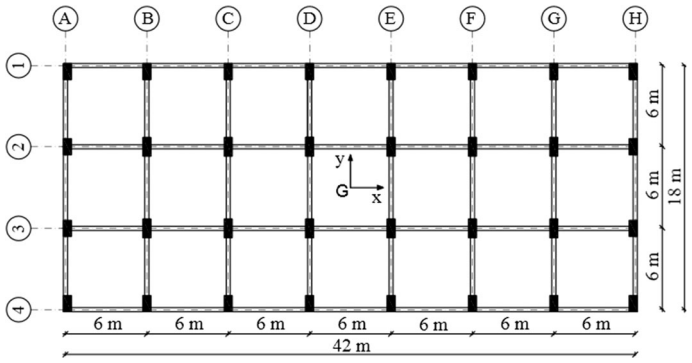

Fig. 15 Typical story plan of the building

6 Application of the "DUVAR" model to an existing structure

The three-story RC building, constructed in the 1970s, consists of seven spans in a longitudinal direction (X) and three spans in a transversal direction (Y). The uniform span lengths are 6 m in two directions. The identical story heights are 4.2 m. While the columns positioned at the façades have sectional dimensions of 30 × 60 cm, all the others have a 30 × 70 cm cross-section. The sectional dimensions of the outer beams are 30 × 80 cm, whereas the inner beams have a section of 30 × 50 cm. The RC slabs have a 15 cm thickness and one can assume that they are infinitely rigid in their own planes.

The structural system involves regular frames with rigid connections. The strong axes of all the columns are parallel on the Y-axis; consequently, the lateral stiffness in each of the two directions is quite different to the other (Fig. 15). The building is used as an office building and located on a firm type of soil.

The equivalent concrete compressive strength, determined by the means of ϕ94 mm cylindrical specimens extracted from the RC members of the structure, is 18 MPa. The longitudinal and lateral reinforcements are mild steel and have a yielding strength of 220 MPa.

The reinforcing details and moment-vs.-curvature relations are illustrated in Figs. 16 and 17.

Although the clay brick infills were not accounted for in the original design phase of the building, beyond their weight and mass, the retrofitted infills were evaluated as structural elements. The bare infills were merely represented by their masses.

The seismic weights calculated for the first two stories of the building were identical and equal to $W_1 = W_2 = 9584$ kN, while the calculation for the top story was $W_3 = 5670$ kN. For the existing conditions, free vibration analyses gave periods of 1.78 and 1.19 s for the X and Y directions, respectively. The mass contribution ratios for the first modes in the X and Y directions were 88 and 84 %, respectively.

The code-based acceleration spectrum used in the evaluation process had corner periods of $T_a = 0.15$ s and $T_b = 0.40$ s. The PGA level was selected as 0.4 g (Turkish Earthquake Code 2007).

The infill walls marked by a gray color in Fig. 18 are retrofitted with CFRP. The total number of retrofitted walls in each story is 16 and the process is repeated in each story.

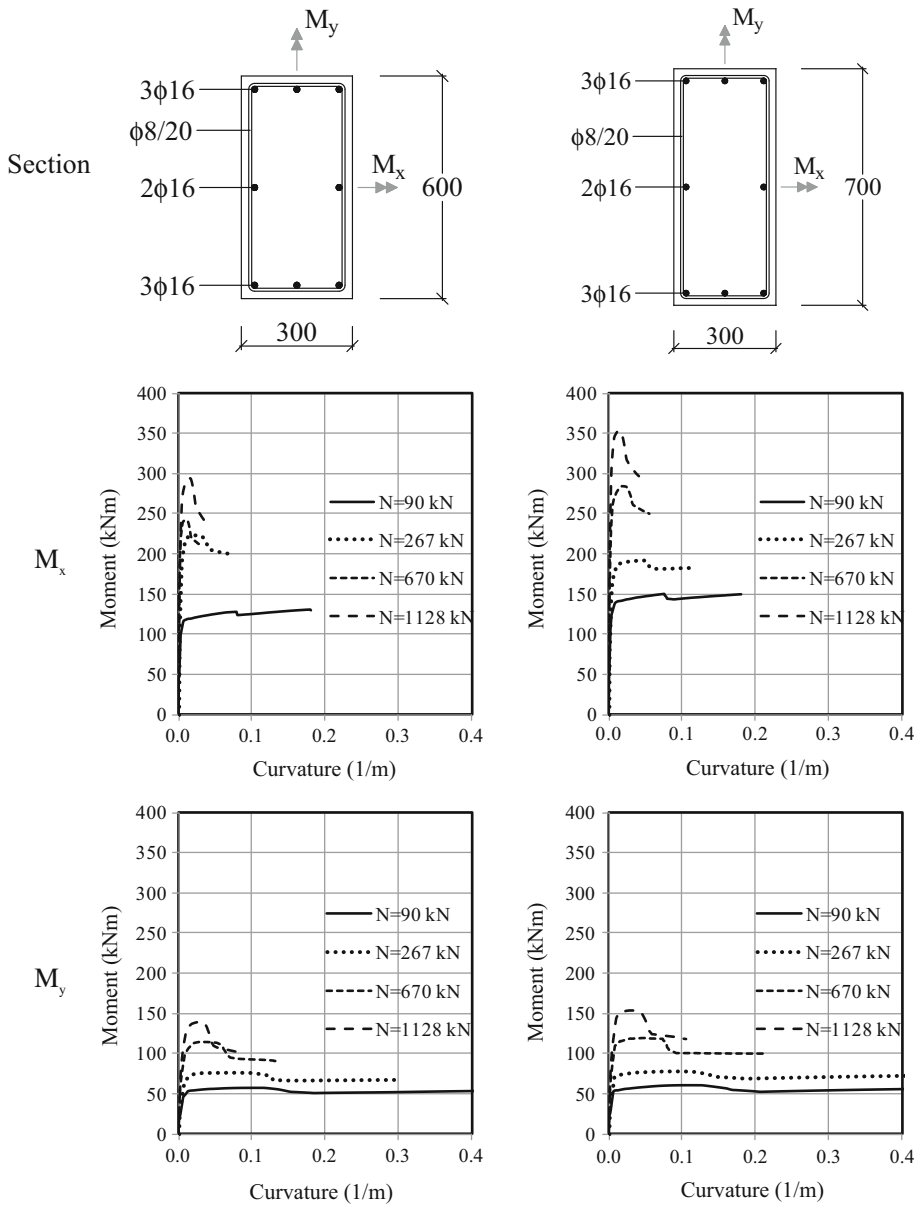

Fig. 16 Column sections and moment-versus-curvature relations

Diamond cross-braced retrofitting has been applied to both sides of the designated walls. The width of the CFRP sheets is 55 cm, and both faces are connected to each other (Fig. 19a). The analytical model of the retrofitted RC frame is illustrated in Fig. 19b. The potential plastic hinges were defined at both ends of the RC members, as well as the nonlinear shear spring used for the retrofitted infill.

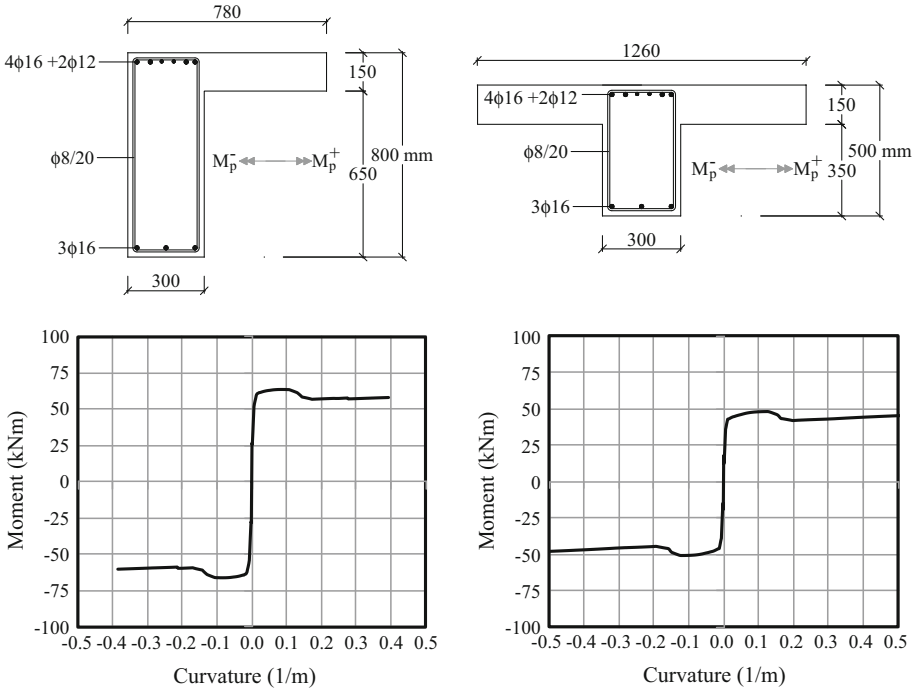

Fig. 17 Beam sections and moment-versus-curvature relations

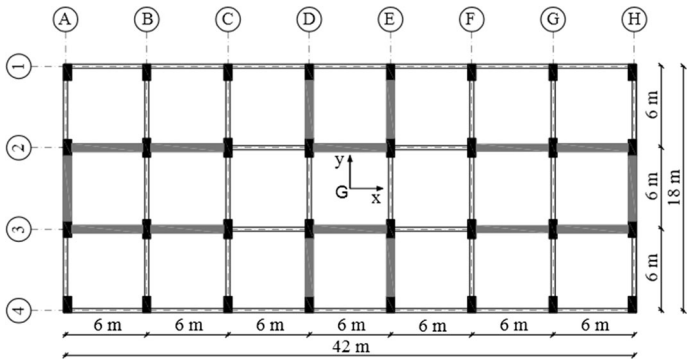

Fig. 18 Position of the retrofitted infill walls on a typical plan

The moment-versus-curvature relations, produced by XTRACT (2006), were assigned to the plastic hinges at both ends of the RC members (Figs. 16, 17, 20). Mander et al. (1998) concrete model and bi-linear steel hardening model were used in the analyses. The load-versus-displacement relations of the retrofitted infills, determined through the "DUVAR" model, are illustrated in Fig. 20.

For the retrofitted case, vibration periods of 0.99 and 0.49 s were obtained in the X and Y directions, respectively. If these values are compared with those of the pre-retrofitting case, it is possible to distinguish the effect of retrofitted infills on the lateral stiffness of the building.

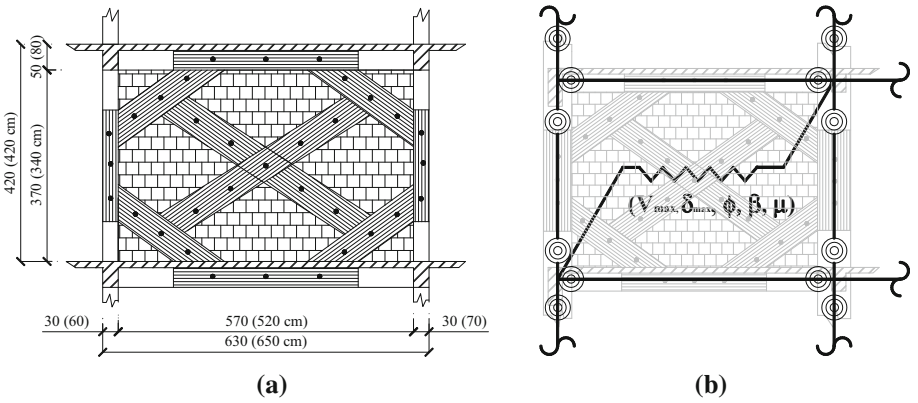

Fig. 19 CFRP retrofitting and the corresponding analytical model. **a** Typical retrofitted detail. **b** Analytical model

Fig. 20 Nonlinear model of the retrofitted infill wall

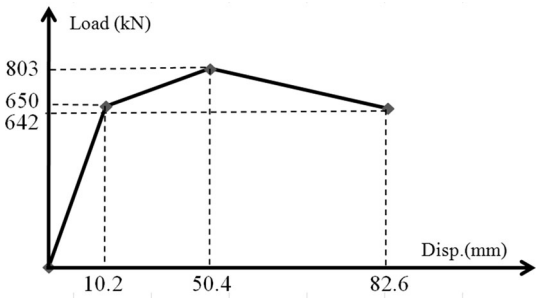

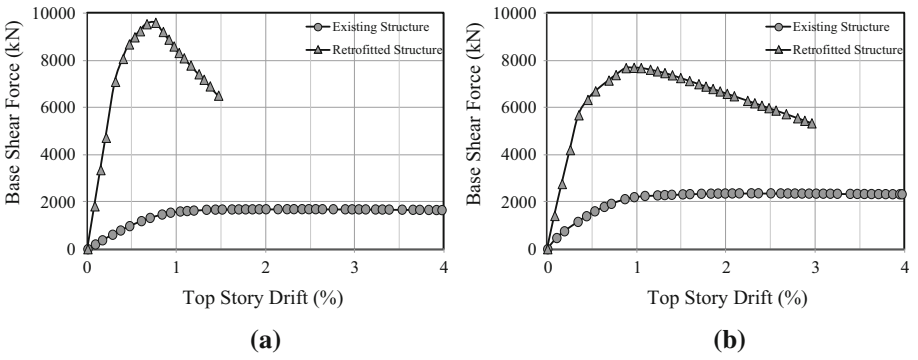

Fig. 21 Capacity curves in two directions. **a** X direction. **b** Y direction

The capacity curves corresponding to the pre- and post-retrofitting cases, extracted from the pushover analyses in which the first-mode-compatible lateral loads are increased monotonically, are presented in Fig. 21.

According to the pushover analyses, the maximum lateral strength in the X and Y directions is 1750 and 2300 kN, respectively, for the pre-retrofitting case. The ultimate displacement is 490 mm for both directions. In the retrofitted case, the maximum lateral

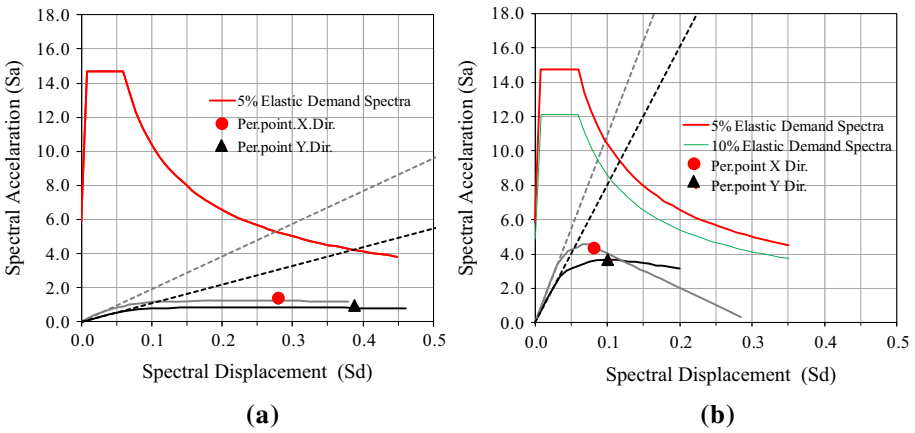

Fig. 22 Demand and capacity curves in Sa–Sd form. **a** Pre-retrofitting case. **b** Post-retrofitting case

Table 13 Performance evaluation in terms of story drifts

Story	Direction	Pre-retrofitting		Post-retrofitting	
		Drifts (%)	Performance level	Drifts (%)	Performance level
3	X	0.7	IO	0.15	IO
	Y	2.3	CP	0.23	IO
2	X	4.4	CP	0.3	IO
	Y	2.8	CP	0.9	IO
1	X	5.0	CP	1.19	IO
	Y	2.6	CP	1.18	IO

strength is 9600 and 7700 kN in the X and Y directions, respectively. The analyses were interrupted when a 20 % strength decrement was observed.

The elastic demand spectra and the capacity curves are presented together in the same spectral era (Fig. 22). Accordingly, the performance points are determined using the procedure defined in FEMA-440 (2005).

For the pre-retrofitting case, spectral displacements were determined as $S_{dx} = 0.390$, $S_{dy} = 0.280$ (Fig. 22a). The corresponding top displacements are 370 and 510 mm in the X and Y directions, respectively.

The seismic demand for the retrofitted case is determined using the elastic demand spectra generated for 10 % critical damping, contingent on Özkaynak et al. (2013). The spectral displacements for the retrofitted case were determined as $S_{dx} = 0.085$ and $S_{dy} = 0.100$ in the two directions. The resultant top displacements are 110 and 130 mm for the X and Y directions, respectively.

FEMA-356 (2000) defines the following performance limits for story drifts: immediate occupancy (IO) 1.0 %, life safety (LS) 2.0 %, and collapse prevention (CP) 4.0 %. The story drift demands of the building corresponding to the performance points are shown in Table 13. With respect to FEMA-356 (2000), although the pre-retrofitting case is in the CP range, the post-retrofitting case is in the IO performance level.

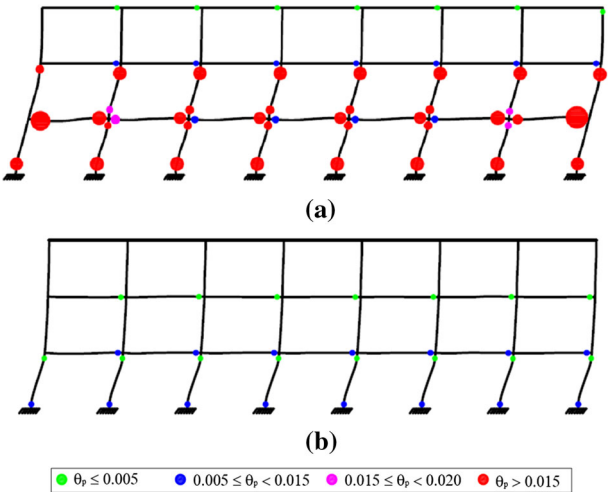

Fig. 23 Plastic hinge distribution of frame '3–3' in X direction. **a** Pre-retrofitting case. **b** Post-retrofitting case

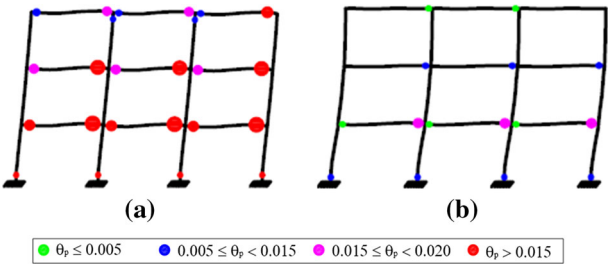

Fig. 24 Plastic hinge distribution of frame 'E–E' in Y direction. **a** Pre-retrofitting case. **b** Post-retrofitting case

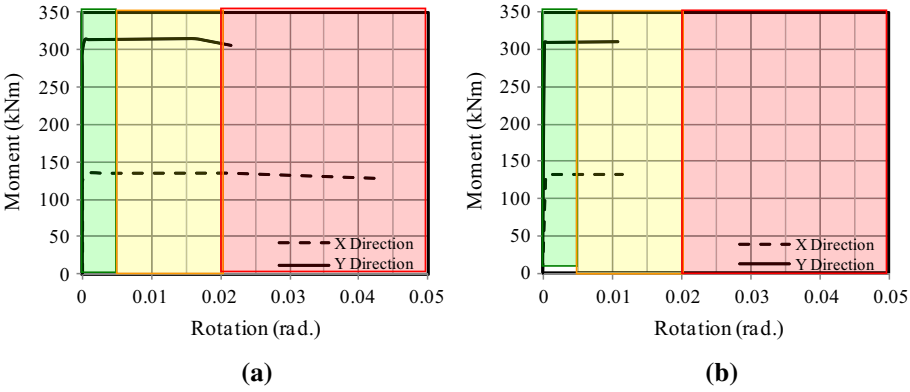

Fig. 25 Moment-vs.-plastic-rotation relations of a B4 column at the first story. **a** Pre-retrofitting case. **b** Post-retrofitting case

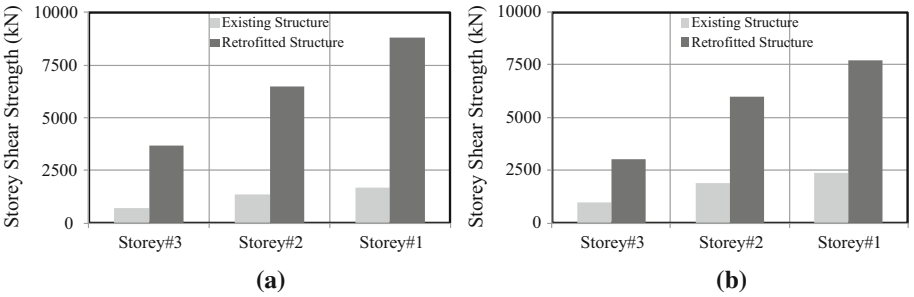

Fig. 26 Story shear capacities. **a** X direction. **b** Y direction

The plastic rotation limits for RC members given in FEMA-356 (2000) are as follows: immediate occupancy (IO) 0.005 rad, life safety (LS) 0.015 rad, and collapse prevention (CP) 0.020 rad. The distribution of the plastic hinges and range of the plastic rotations are illustrated in Fig. 23. The colored circles with different diameters indicate the magnitude and performance range of the hinge. In the pre-retrofitting case, many columns in the first and second story, especially in their weak directions, reached *collapse state* in addition to the observed beam damages (Figs. 23a, 24a). After retrofitting, the damages of columns and beams decreased significantly in both directions (Figs. 23b, 24b). The new performance level is in the IO range.

The typical B4 column is assessed at the first story in terms of its plastic rotation demands (Fig. 25). Although the column reaches the CP range in both directions for the pre-retrofitting case, it remains in the IO range in both directions for the post-retrofitting case.

The story shear capacities corresponding to pre- and post-retrofitting cases are presented in Fig. 26a, b.

In post-retrofitting case, the story shear capacities increase more than 100 % compared with pre-retrofitting case. Moreover, in the retrofitted case the story shear strengths rise gradually from top to bottom.

7 Conclusions

The following conclusions can be drawn:

1. An empirical behavior model for bare and CFRP-based retrofitted infills was proposed.
2. The proposed "DUVAR" model was evaluated using the different existing experimental results. The model was successful enough to predict the initial stiffness, maximum shear strength and descending branch.
3. The proposed model was utilized in the analysis of an existing 3D RC structure to be retrofitted. The earthquake performance evaluation, made with respect to FEMA-356 (2000), yielded the results that the CFRP-based retrofitting on the infill walls led to rigorous performance increments.
4. According to the story drifts and sectional plastic rotation demands of the three-story building, the CFRP-based retrofitting was exceedingly effective in the performance improvement of the existing structure.

5. The performed pushover analysis of the three-story building showed that the CFRP-based retrofitting of the existing infills is capable of increasing the stiffness and strength capacities of the structure without the need to use any other retrofitting techniques.

Acknowledgments This paper was sponsored by research projects 106M050 of the Scientific and Technological Research Council of Turkey (TUBITAK) and 31966 of Istanbul Technical University (ITU) Research Funds. The contributions of Prof. Dr. Oral Büyüköztürk, Assoc. Prof. Dr. Cem Yalçın and Ass. Prof. Dr. A. Anıl Dindar to this paper are gratefully acknowledged.

References

Almusallam TH, Al-Salloum YA (2007) Behavior of FRP strengthened infill walls under in-plane seismic loading. J Compos Constr (ASCE) 11(3):308–318

Altın S, Anıl Ö, Kara ME (2008a) Strengthening of RC nonductile frames with RC infills: an experimental study. Cem Concr Compos 30(7):612–621

Altın S, Anıl Ö, Kara ME, Kaya M (2008b) An experimental study on strengthening of masonry infilled RC frames using diagonal CFRP strips. Compos B Eng J 39(4):680–693

American Society of Civil Engineers (ASCE) (2007) Seismic rehabilitation of existing buildings (ASCE/SEI 41-06). ASCE, Reston, VA

Anıl Ö, Altın S (2007) An experimental study on reinforced concrete partially infilled frames. Eng Struct 29(3):449–460

Canadian Standards Association (CSA) (2004). Design of masonry structures (S304.1-04). CSA, Ontario

Chrysostomou CZ, Gergely P, Abel JF (1992). Nonlinear seismic response of infill steel frames. In: Proceedings of the 10th world conference on earthquake engineering, Madrid, Spain, vol 8, pp 4435–4437

Dhanasekhar M, Page AW (1986) The influence of brick masonry infill properties on the behaviour of infilled frames. ICE Proc 81(4):593–605

Dolšek M, Fajfar P (2008) The effects of masonry infills on the seismic response of a four-storey reinforced concrete frame a deterministic assessment. Eng Struct 30(7):1991–2001

Erdem I, Akyüz U, Ersoy U, Özcebe G (2006) An experimental study on two different strengthening techniques for RC frames. Eng Struct 28(13):1843–1851

Erkoseoglu G, Erberik MA, Cıtıloglu C (2014). A parametric study on unreinforced and confined masonry wall behavior. In: Second European conference on earthquake engineering and seismology, Istanbul, Turkey

FEMA-356 (2000) Prestandard and commentary for the seismic rehabilitation of buildings. Prepared by the American Society of Civil Engineers (ASCE), Reston, VA, for the Federal Emergency Management Agency (FEMA), Washington, DC

FEMA-440 (2005) Improvement of nonlinear static seismic analysis procedures. Prepared by ATC for the American Society of Civil Engineers (ASCE), for the Federal Emergency Management Agency (FEMA), Washington, DC

Hashemi A, Mosalam KM (2006) Shake-table experiment on reinforced concrete structure containing masonry infill wall. Earthq Eng Struct Dyn 35(14):1827–1852

Holmes M (1961) Steel frames with brickwork and concrete infilling. ICE Proc 19(4):473–478

Kakaletsis DJ, Karayannis CG (2009) Experimental investigation of infilled reinforced concrete frames with openings. ACI Struct J 106(2):132–141

Karadoğan F, Yüksel E, İlki A (2003). Structural behavior of ordinary RC bare and brittle partitioned frames with and without lap splice deficiency. In: Wasti ST, Özcebe G (eds.) Seismic assessment and rehabilitation of existing buildings: proceedings of the NATO science for peace workshop on seismic assessment and rehabilitation of existing buildings, İzmir, Turkey

Madan A, Reinhorn AM, Mander JB, Valles RE (1997) Modeling of masonry infill panels for structural analysis. J Struct Eng 123(10):1295–1302

Mainstone RJ (1971) On the stiffness and strengths of infilled frames. Proceedings Institution of Civil Engineers, Suppl (iv): 57–90

Mander JB, Priestley MJN, Park R (1998) Theoretical stress–strain model for confined concrete. J Struct Eng (ASCE) 114(8):1804–1826

Masonry Standards Joint Committee (MSJC) (2011). Building code requirements for masonry structures (TMS 402-11/ACI 530-11/ASCE 5-11). The Masonry Society, American Concrete Institute, and the American Society of Civil Engineers, Boulder, Farmington Hills, and Reston

Mosalam KM (1996). Experimental and computational strategies for the seismic behavior evaluation of frames with infilled walls. PhD Thesis, Cornell University. Ithaca, NY

Mosalam KM, White RN, Ayala G (1998) Response of infilled frames using pseudo-dynamic experimentation. Earthq Eng Struct Dyn 27(6):589–608

New Zealand Society for Earthquake Engineering Inc. (NZSEE) (2006) Assessment and improvement of the structural performance of buildings in earthquakes: recommendations of a NZSEE study group on earthquake risk buildings June 2006, Including Corregendum No 1. NZSEE, Wellington

Özcebe G, Ersoy U, Tankut T, Erduran E, Keskin RSO, Mertol HC (2003) Strengthening of brick-infilled RC frames with CFRP (Rep no. 2003/1). Structural Engineering Research Unit (SERU). TUBITAK-METU, Ankara

Özkaynak H, Yüksel E, Büyüköztürk O, Yalçın C, Dindar AA (2011) Quasi-static and pseudo-dynamic testing of infilled RC frames retrofitted with CFRP material. Compos B Eng J 42(2):238–263

Özkaynak H, Yüksel E, Yalçın C, Dindar AA, Büyüköztürk O (2013) Masonry infill walls in reinforced concrete frames as a source of structural damping. Earthq Eng Struct Dyn 43(7):949–968

Polyakov SV (1960) On the interaction between masonry filler walls and enclosing frame when loaded in the plane of the walls. Translation in earthquake engineering. Earthquake Engineering Research Institute, San Francisco, pp 36–42

Pujol S, Fick D (2010) The test of a full-scale three-story RC structure with masonry infill walls. Eng Struct 32(10):3112–3121

Saatcioglu M (2003) Research on seismic retrofit and rehabilitation of reinforced concrete structures. In: Proceedings of the 31st annual conference of the Canadian society for civil engineering (CSCE), pp 1500–1510

Saneinejad A (1990). Non-linear analysis of infilled frames. PhD Thesis, Department of Civil Engineering and Structural Engineering, University of Sheffield

Saneinejad A, Hobbs B (1995) Inelastic design of infilled frames. J Struct Eng (ASCE) 121(4):634–650

SAP2000 v12. Structural analysis program. Computer and Structures Inc., Berkeley, CA

Shing PB, Lotfi HR (1991) Experimental and finite element analyses of single-story reinforced masonry shear walls. In: Middleton MJ, Pande GN (eds) Computer methods in structural masonry. Books and Journals International, Swansea, pp 74–83

Smith BS, Carter C (1969) A method of the analysis for infilled frames. ICE Proc 44(1):31–48

Smyrou E, Blandon C, Antoniou S, Pinho R, Crisafulli F (2011) Implementation and verification of a masonry panel model for nonlinear dynamic analysis of infilled RC frames. Bull Earthq Eng 9:1519–1534

Triantafillou TC (1998) Strengthening of masonry structures using epoxy-bonded FRP laminates. J Compos Constr 2(2):96–104

Turkish Earthquake Code (2007) Ankara ministry of public works. Ankara

XTRACT v3.0.7 (2006) Cross-sectional structural analysis of components. Imbsen Software Systems, Sacramento, CA

Yüksel E, Özkaynak H, Büyüköztürk O, Yalçın C, Dindar AA, Sürmeli M, Taştan D (2009) Performance of alternative CFRP retrofitting schemes used in infilled RC frames. Constr Build Mater 24:596–609

Žarnic R, Gostic S (1997) Masonry infilled frames as an effective structural sub-assemblage. In: Fajfar P, Krawinkler H (eds) Seismic design methodologies for the next generation of codes. Balkema, Rotterdam, pp 335–346